Extremely High Sea Surface Temperatures in 2023

Boyin Huang[1], Xungang Yin[1], James A. Carton[2], Ligang Chen[2], Garrett Graham[3], Patrick Hogan[1], Thomas Smith[4], Huai-Min Zhang[1]

[1] NOAA/NCEI, Asheville, North Carolina

[2] Dept. Atmos. Oceanic Science, Univ. Maryland, College Park, Maryland

[3] North Carolina Institute for Climate Studies, North Carolina State University, Asheville, North Carolina

[4] NOAA/Center for Satellite Applications and Research, College Park, Maryland

Corresponding author address: boyin.huang@noaa.gov

Abstract

NOAA's Daily Optimum Interpolation Sea Surface Temperature (DOISST) indicates that globally averaged sea surface temperature (SST) broke record in March 2023 and set new record highs in April, July, and August 2023. This has raised intense media interest and public concern about causes and connections to climate change. Our analysis indicates that the record high SSTs qualified as marine heatwaves (MHWs) and even super-MHWs as defined in this study, and are attributed to three factors: (i) a linear trend, (ii) a shift to the warm phase of the multi-decadal Pacific-Atlantic-Arctic Oscillation (PAO) pattern which is identified in this study, and (iii) the transition from the triple-dip succession of La Niña events to the 2023 El Niño event.

One-Sentence Summary

The extreme warm SSTs in 2023 resulted from linear warming trends, a pattern of low-frequency oscillation, and the El Niño event.

1. Introduction

NOAA's DOISST version 2.1 (v2.1) (1) indicates that globally (90ºS−90ºN) averaged SST set a new daily record of 18.83ºC on April 4, 2023 (Fig. 1). This broke the previous global record (18.78ºC) set on March 6, 2016, which occurred during the historically strong 2015−16 El Niño event (2, 3). An unusual feature of the record-breaking SST in April 2023 is that it happened immediately after the triple-dip 2020−23 succession of La Niña events (4), during which tropical Pacific SSTs were relatively low. Usually, record high SSTs occur during or soon after El Niño events, such as in August 27, 2015 (18.66ºC) and March 6, 2016 (18.78ºC; Fig. 1). The globally averaged SST continued to increase in July and August 2023 as the 2023−24 El Niño event intensified, and new daily records were set numerous times during July and August 2023. These record-breaking SSTs raised intense media and public interest in their causes and concern about the consequences of MHWs (5, 6) for the marine environment and implications for extreme weather and longer term climate change. This study reviews the evolution of the record-breaking SSTs in 2023 and discusses the reasons for the extremely high SSTs.

2. Results

2.1 Extreme SSTs

As shown in Figure 1, the globally averaged SST in DOISST reached a record high on April 4, 2023 (18.83ºC). This record was broken again in mid-July and reached a new record high on August 21 (19.00ºC). After removing the climatological daily SST at each spatial location (computed over 1982−2011), we see that the globally averaged daily SST anomaly (SSTA; 0.81ºC) on the latter date is about 5 times the standard deviation (σ=0.16ºC), which exceeds the expected daily climatological value at the 99% significance level. Overall, the SSTs in August 2023 were extremely high and are the focus of this study.

The extremely high SSTAs during August 2023 are distributed globally. The average SSTAs were high in the tropical Pacific (1º−3ºC), the North Pacific north of 30ºN (2º−6ºC), the North Atlantic (2º−5ºC), the Arctic coastal zone (2º−6ºC), the tropical Indian Ocean (1ºC), and the Southern Ocean (1º−2ºC) (Fig. 2a). These high SSTAs manifest strong MHWs (Fig. 2b), defined by the criterion of SSTAs higher than the 90th percentile. The MHW intensity in the accumulative SSTAs in units of degree-day (DD) is clearly seen in the tropical Pacific (20−100 DD), the North Pacific

north of 30ºN (20−150 DD), the North Atlantic (20−100 DD), the Arctic coastal zone (>150 DD), the tropical Indian Ocean west of 90ºE (20 DD), and the Southern Ocean (20−50 DD).

The extreme magnitude of the SST in August 2023 is highlighted by the prevalence of super-MHWs, which occur when SSTs at that spatial location break the historic year-day record. Figure 2c clearly shows such super-MHWs occurring in the central tropical Pacific near the dateline (0.1º−0.2ºC), the eastern tropical Pacific east of 120ºW (0.1º−0.5ºC), the North Pacific north of 30ºN (0.2º−1.0ºC), the northern tropical Atlantic between the equator and 30ºN (0.2º−0.5ºC), the northwestern North Atlantic south of Greenland (0.5ºC), the Arctic coastal zone (0.5º−2.0º), the western Indian Ocean west of 90ºE (0.2º−1.0ºC), and the Southern Ocean (0.2º−1.0ºC).

3.2 Reasons for the extreme SST

The question is, what caused the extreme SSTs in August 2023? We address this question by examining a decomposition of SSTA into three components: a linear trend, and two SST patterns derived from the empirical orthogonal function (EOF) analysis (7): EOF1 for El Niño and Southern Oscillation (ENSO) (8) and EOF2 for PAO.

Using the NOAA monthly Extended Reconstructed SST version 5 (ERSSTv5) (9), the SST linear trends over 1950−2023 were calculated (Fig. 3a), which show overall SST warming over almost the entire global oceans. In particular, the SST trends are high in the tropical Indian Ocean and western Pacific (0.10º−0.15ºC per decade; ºC/dec), the western-central South Pacific over 30ºS−50ºS (0.10º−0.15ºC/dec), the Bering Sea (0.25ºC/dec), the northwestern North Atlantic (0.25ºC/dec), the tropical Atlantic (0.10º−0.20ºC/dec), the western South Atlantic (0.25ºC/dec), and the Arctic coastal zone (0.25ºC/dec). The pattern of these SST trends is, to some degree, similar to that of SSTAs shown in Figure 2a. For example, both SSTAs and SST trends were high in the North Atlantic, particularly the northwestern North Atlantic. To explore the contribution of this persistent SST warming trend to the extreme SSTs of 2023, the linear trend of SSTs computed at each location was removed and the detrended SSTA was computed. The globally averaged SSTAs with and without trends are compared in Fig. 3b. This comparison clearly shows that the high SSTAs in the 2010s were largely a result of this long-term warming trend. In August 2023 the global average SSTA decreased from +0.7ºC to +0.4ºC after this detrending.

The detrended global SSTAs were then decomposed into EOF1, EOF2, and their associated principal components PC1 and PC2. The EOF1 (Fig. 3c) represents a typical ENSO pattern, whose magnitude fluctuates between 3−7 years (8) seen in PC1 (Fig. 3d). The EOF1 explains 17% of the detrended SSTA variance, with large contributions from the central-eastern tropical Pacific, eastern North Pacific, the central South Pacific south 40ºS, and the western tropical Indian Ocean. Indeed, the globally averaged SSTA after detrending is clearly associated with ENSO activities represented by PC1 or commonly the Niño3.4 index (10). The lag-1 correlation coefficient between the detrended SSTA and Niño3.4 index (Fig. 3b) is 0.61, which is significant at the 99% level.

The EOF2, which is defined as PAO in this study, was identified in the North Pacific north of 30ºN, the North Atlantic north of 20ºN, and the Arctic coastal zone (Fig. 3e), which explains 6% of the detrended SSTA variance. As shown in Figure 3f, the PAO period is about 70 years, and was in its warm phase in the 1950s−60s, cold phase in the 1970s−90s, and warm phase again in the 2010s−20s. The PAO is similar to the Atlantic Multidecadal Oscillation (AMO) (11, 12), but with a broader spatial distribution across three ocean basins. The spatial distribution of PAO north of 30ºN is very similar to the patterns of the high SSTAs observed in August 2023 in Figure 2a, and the warm phase of PAO after the 2010s matches the strong warming in 2023. This distribution and coincidence with high SSTs suggest a close relationship between PAO and the extremely high SSTs in 2023.

The connection between the phase of the PAO and the extreme SSTAs in the PAO regions is shown by the averaged SSTAs in the North Pacific north of 30ºN (Fig. 4a), the North Atlantic over 30ºN−60ºN (Fig. 4b), and the Arctic coastal zone over 60ºN−80ºN (Fig. 4c). It is clear that, when the SST linear trends were subtracted out, the averaged SSTAs are greatly reduced in the North Pacific after the 2010s and in the North Atlantic and the Arctic coastal zone after the 2000s. These SSTAs are further reduced when the projection onto the PAO pattern is removed. On average (1950−2023), the SSTA variances over 30ºN−80ºN decrease by 39%, 32%, and 3%, respectively, due to detrending and removing PAO and ENSO projections (Table S1). In contrast, the variances in the global oceans over 90ºS−90ºN decrease by 83%, 5%, and 6%, respectively, indicating the dominant role of linear trend in global SST warming.

It is interesting to note that clear seasonal fluctuation can be seen in PC2 (Fig. 3f) and the Arctic SSTAs (Fig. 4c) after the 2000s, which peak in the boreal summer (July−September) and plunge in boreal winter (January−March). This suggests that the role of PAO in the SSTs in the PAO region is particularly strong during boreal summer, while its role is relatively weak during boreal winter. The reason for the seasonal fluctuations of PAO may result from more and denser in situ observations from buoys and Argo floats after the 2000s, as well as more ship observations in boreal summer, which may better resolve the seasonal variation of SSTs.

The monthly SSTs in August 2023 are displayed in Figure 5 when (i) the linear trends, (ii) the PAO pattern (EOF2), and (iii) the ENSO mode (EOF1) are successively subtracted. The original SSTAs (Fig. 5a) are high in central-eastern tropical Pacific (1º−3ºC), the North Pacific (2º−3ºC) north of 30ºN, the North Atlantic (1º−2ºC), the Arctic coastal zone (1º−3ºC), the western Indian Ocean (1ºC), and the South Pacific east of New Zealand (1ºC). After removing the linear trends (Fig. 5b), these SSTAs are reduced by about 0.5ºC in those regions except for the tropical Pacific where linear trends are small as shown in Figure 3a. After further removing PAO pattern (Fig. 5c), SSTs are further reduced by about 0.5º−1.0ºC in the North Pacific north of 30ºN, the North Atlantic, and the Arctic coastal zone. When the ENSO mode is removed (Fig. 5d), the SSTAs in the central-eastern tropical Pacific is reduced by 0.5º−1.0ºC, but part of the SSTA remains in the east due to the existence of ENSO influence not represented by the first ENSO mode. The globally averaged SSTA variances are 0.59, 0.48, 0.34, and 0.29 K^2 in Figures 5(a)−(d), respectively, indicating clear contributions of the linear trends (19%), PAO (24%), and ENSO (8%) to the extremely high SSTs in August 2023.

3. Summary and Discussion

The SST analyses based on NOAA's DOISST show that globally (90ºS−90ºN) averaged daily SSTs were at record high on 4 April 2023 (18.83ºC), and the record was continually broken since 16 July until a new record reached on 21 August 2023 (19.00ºC). These record high SSTs were the result of extremely high SSTs in the tropical Pacific, the North Pacific north of 30ºN, the North Atlantic, the Arctic coastal zone, the tropical Indian Ocean, and the Southern Ocean. The SST extremes resulted in MHWs (defined by SSTAs exceeding the 90th percentile) and even resulted in some super-MHWs, defined as SSTAs above 100th percentile in these regions. Our analyses indicate that the extremely high SSTs in the summer of 2023 results from three overlapping

contributors: the long-term linear warming trends that other studies have associated it with increasing greenhouse gases (13); the warming phase of a broad multidecadal PAO pattern after the 2010s which is most pronounced in the boreal summer; and finally the warming due to the transition from the cool conditions associated with the triple-dip La Niña (2000−23) to warm conditions of El Niño (2023−24).

The record high SSTs over 2015 and 2023 in DOISST were consistent with those similar SST data sets, including OSTIA and CMC (Fig S1), although subtle differences were found among them. For example, in March 2023, a new record SST was found in DOISST but not in OSTIA and CMC. These differences largely result from different algorithms for ship bias correction, satellite bias correction, and different spatial resolutions (14). The linear trends and EOFs were analyzed using monthly ERSSTv5 from 1950 to 2023, when SST data are more reliable. However, the analysis of ERSSTv5 from 1900 to 2023 resulted in very similar ENSO and PAO patterns and their associated PCs (Fig. S2), in which the period of PAO may be estimated more accurately. In addition, the modes of ENSO and PAO based on ERSSTv5 over 1950−2023 are consistent with those in the independent data set HadISST over 1950−2022 (Fig. S3). In conclusion, the results shown in this study are consistent across different data sets and for analyses over different time periods. The SSTs over the global oceans in 2023 is extremely high; and the extremely high SSTs resulted from a combination of trends, PAO, and ENSO.

References

1. B. Huang, C. Liu, V. Banzon, E. Freeman, G. Graham, B. Hankins, T. Smith, and H.-M. Zhang, Improvements of the Daily Optimum Interpolation Sea Surface Temperature (DOISST) Version 2.1. J. Climate, 34, 2923-2939 (2021). DOI 10.1175/JCLI-D-20-0166.1

2. B. Huang, M. L'Heureux, Z.-Z. Hu, and H.-M. Zhang, Ranking the strongest ENSO events while incorporating SST uncertainty. Geophys. Res. Lett., 43 (2016). doi:10.1002/2016GL070888

3. M. L. L'Heureux, K. Takahashi, A. B. Watkins, A. G. Barnston, E. J. Becker, T. E. Di Liberto, F. Gamble, J. Gottschalck, B. Huang, K. Mosquera-Vasquez, and A. T. Wittenberg,

Observing and Predicting the 2015-16 El Nino. Bull. Amer. Meteor. Soc. , September 2017, 1363-1382 (2017). doi:10.1175/BAMS-D-16-0009.1

4. X. Li, Z.-Z. Hu, M. J. McPhaden, C. Zhu, and Y. Liu, Triple-Dip La Niñas in 1998-2001 and 2020-2023: Impact of Mean State Changes. J. Geophys. Res., 128 (17), e2023JD038843 (2023). DOI: 10.1029/2023JD038843

5. A. J. Hobday, Alexander, L. V., Perkins, S. E., Smale, D. A., Straub, S. C., Oliver, E. C. J., et al., A hierarchical approach to defining marine heatwaves. Progress in Oceanography, 141, 227–238 (2016). https://doi.org/10.1016/j.pocean.2015.12.014

6. B. Huang, Z. Wang, X. Yin, A. Arguez, G. Graham, C. Liu, T. Smith, H.-M. Zhang, Prolonged Marine Heatwaves in the Arctic: 1982-2020. Geophys. Res. Lett., 48, e2021GL095590 (2021). https://doi.org/10.1029/2021GL095590

7. J. E. Kutzbach, Empirical eigenvectors of sea-level pressure, surface temperature and precipitation complexes over North America. J. Appl. Meteor., 6, 791-802 (1967).

8. S. G. Philander, El Niño, La Niña, and the southern oscillation. International geophysics series, 46, pp.X-289 (1989).

9. B. Huang, P. W. Thorne, V. F. Banzon, T. Boyer, G. Chepurin, J. H. Lawrimore, M. J. Menne, T. M. Smith, R. S. Vose, and H.-M. Zhang, Extended Reconstructed Sea Surface Temperature version 5 (ERSSTv5), Upgrades, validations, and intercomparisons. J. Climate, 30, 8179-8205 (2017). doi:10.1175/JCLI-D-16-0836.1

10. S. E. Zebiak, and M. A. Cane, A model El Niño–Southern Oscillation. Mon. Wea. Rev., 115, 2262–2278 (1987). https://doi.org/10.1175/1520-0493(1987)115,2262:AMENO.2.0.CO;2

11. M. E. Schlesinger, and N. Ramankutty, An oscillation in the global climate system of period 65–70 years. Nature, 367(6465), pp.723-726 (1994).

12. R. A. Kerr, A North Atlantic climate pacemaker for the centuries. Science, 288(5473), 1984-1985 (2000).

13. G. Schmidt, D. Shindell, and K. Tsigaridis, Reconciling warming trends. Nature Geosci 7, 158–160 (2014). https://doi.org/10.1038/ngeo2105

14. B. Huang, X. Yin, J. A. Carton, L. Chen, G. Graham, C. Liu, T. Smith, H.-M. Zhang, Understanding Differences in Sea Surface Temperature Intercomparisons. JTECH, 40, 455-473 (2023). DOI 10.1175/JTECH-D-22-0081.1

15. A. Ignatov, X. Zhou, B. Petrenko, X. Liang, Y. Kihai, P. Dash, J. Stroup, J. Sapper, and P. DiGiacomo, AVHRR GAC SST Reanalysis Version 1 (RAN1). Remote Sensing, 8, 315 (2016). https://doi.org/10.3390/rs8040315

16. S. Good, and Coauthors, The current configuration of the OSTIA system for operational production of foundation sea surface temperature and ice concentration analyses. Remote Sens., 12, 720 (2020). https://doi.org/10.3390/rs12040720

17. B. Brasnett, and D. S. Colan, Assimilating retrievals of sea surface temperature from VIIRS and AMSR2. J. Atmos. Oceanic Technol., 33, 361–375 (2016). https://doi.org/10.1175/JTECH-D-15-0093.1

18. N. A. Rayner, D. E. Parker, E. B. Horton, C. K. Folland, L. V. Alexander, D. P. Rowell, E. C. Kent, and A. Kaplan, Global analyses of sea surface temperature, sea ice, and night marine air temperature since the late nineteenth century. J. Geophys. Res., 108, 4407 (2003). doi:10.1029/2002JD002670

Acknowledgments:

Authors thank Rost Parsons, Scott Cross and Zhankun Wang for their precious comments on this study. The opinions expressed in this paper are those of the authors alone and do not necessarily reflect official NOAA, Department of Commerce, or U.S. government policy. JAC and LC were supported by the NOAA Climate Program Office (NA20OAR4310339).

Author contributions:

Methods: BH, XY

Visualization: BH, XY

Writing: BH, XY, TS, JAC, GG, ZH, PH

Weekly discussion: BH, XY, TS, JAC, GG, ZH, LC

Competing interests:

Authors declare that they have no competing interests.

Data and material availability:

Data sets used in this study are available: https://www.ncei.noaa.gov/data/sea-surface-temperature-optimum-interpolation/v2.1 for DOISST v2.1,

https://www.ncei.noaa.gov/products/extended-reconstructed-sst for ERSSTv5,
https://podaac.jpl.nasa.gov/dataset/CMC0.1deg-CMC-L4-GLOB-v3.0 for CMC SST,
https://podaac.jpl.nasa.gov/dataset/OSTIA-UKMO-L4-GLOB-v2.0 for OSTIA SST, and
https://www.metoffice.gov.uk/hadobs/hadisst for HadISST.

Data for Figures 1−5 and S1−S3 and Table S1 are available at
https://www.ncei.noaa.gov/pub/data/cmb/ersst/v5/2023.science/

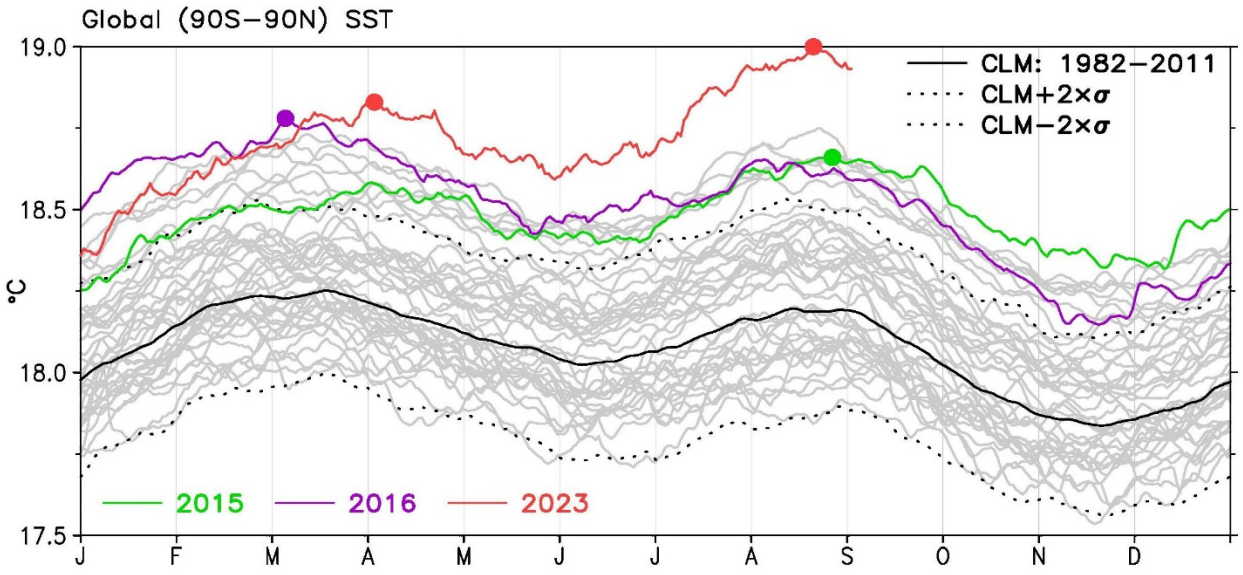

Fig. 1. Globally (90ºS−90ºN) averaged SST from 1982 to 2023 represented by gray lines except for 2015 (solid green), 2016 (solid purple), and 2023 (solid red). The new SST records were noted with solid circles on 27 August 2015, 6 March 2016, 4 April 2023, and 21 August 2023. The 1982−2011 climatology (CLM) and its two standard deviation (2σ) intervals are expressed by solid and dotted black lines. Data source: DOISST v2.1.

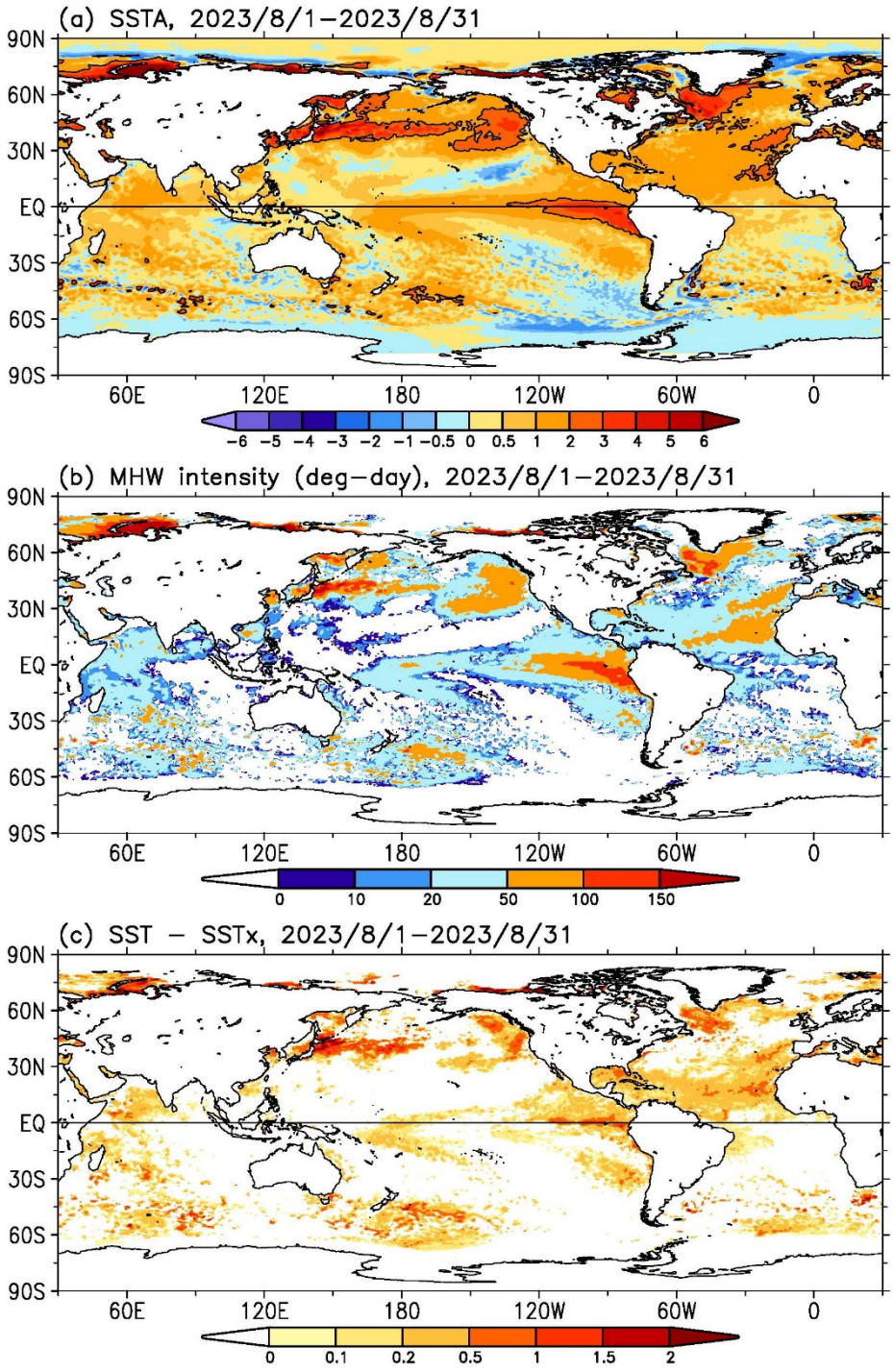

Fig. 2. Extreme SSTAs in August 2023 expressed in (a) average SSTAs (ºC) in reference of the 1971−2000 climatology, (b) conventional MHW intensity index in units of degree-day, and (c) super-MHW intensity (ºC) of average SST difference in reference of the maximum SST (SSTx) over 1982−2022. The contour 2ºC is highlighted in (a). Data source: DOISST v2.1.

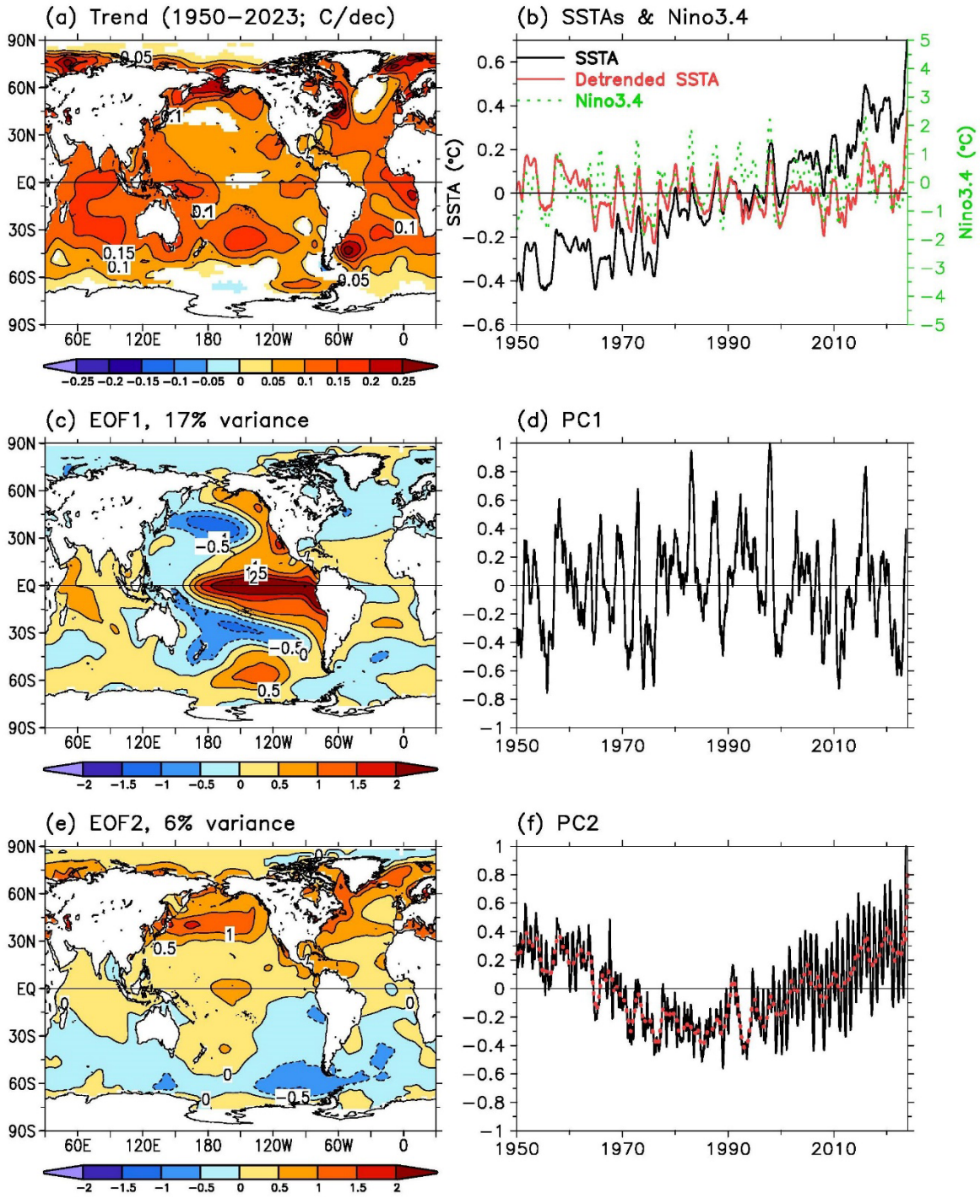

Fig. 3. (a) SSTA trends (ºC per decade) over 1950−2023, (b) Globally averaged SSTA (solid black), detrended SSTA (solid red), and Niño3.4 index (dotted green; right y-axis), (c) EOF1, (d) PC1, (e) EOF2, and (f) PC2 of the detrended monthly SSTA. Trends with significance level lower than 95% have been masked out in (a). Lines in (b) are filtered with a 7-month filter, and a line (dotted red) with a 12-month filter is overlapped in (f). Data source: ERSSTv5.

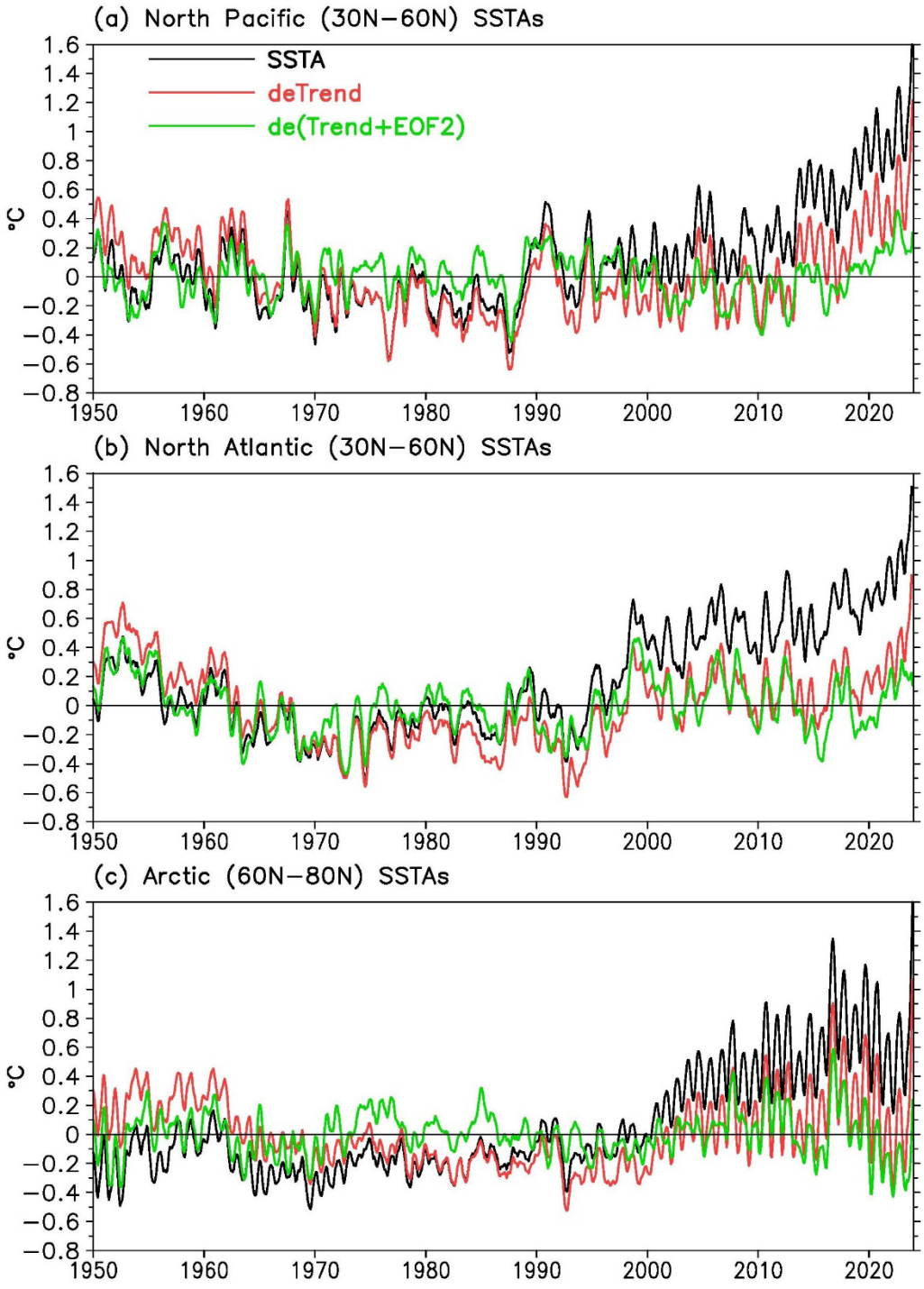

Fig. 4. Averaged SSTA (ºC; solid black), SSTAs after removing trend (deTrend; solid red), and removing trend and EOF2 [de(Trend+EOF2); solid green] in (a) the North Pacific (30ºN−60ºN), (b) the North Atlantic (30ºN−60ºN), and (c) the Arctic (60ºN−80ºN). A 7-month filter is applied when plotting. Their average (1950−2023) variances are listed in Table S1. Data source: ERSSTv5.

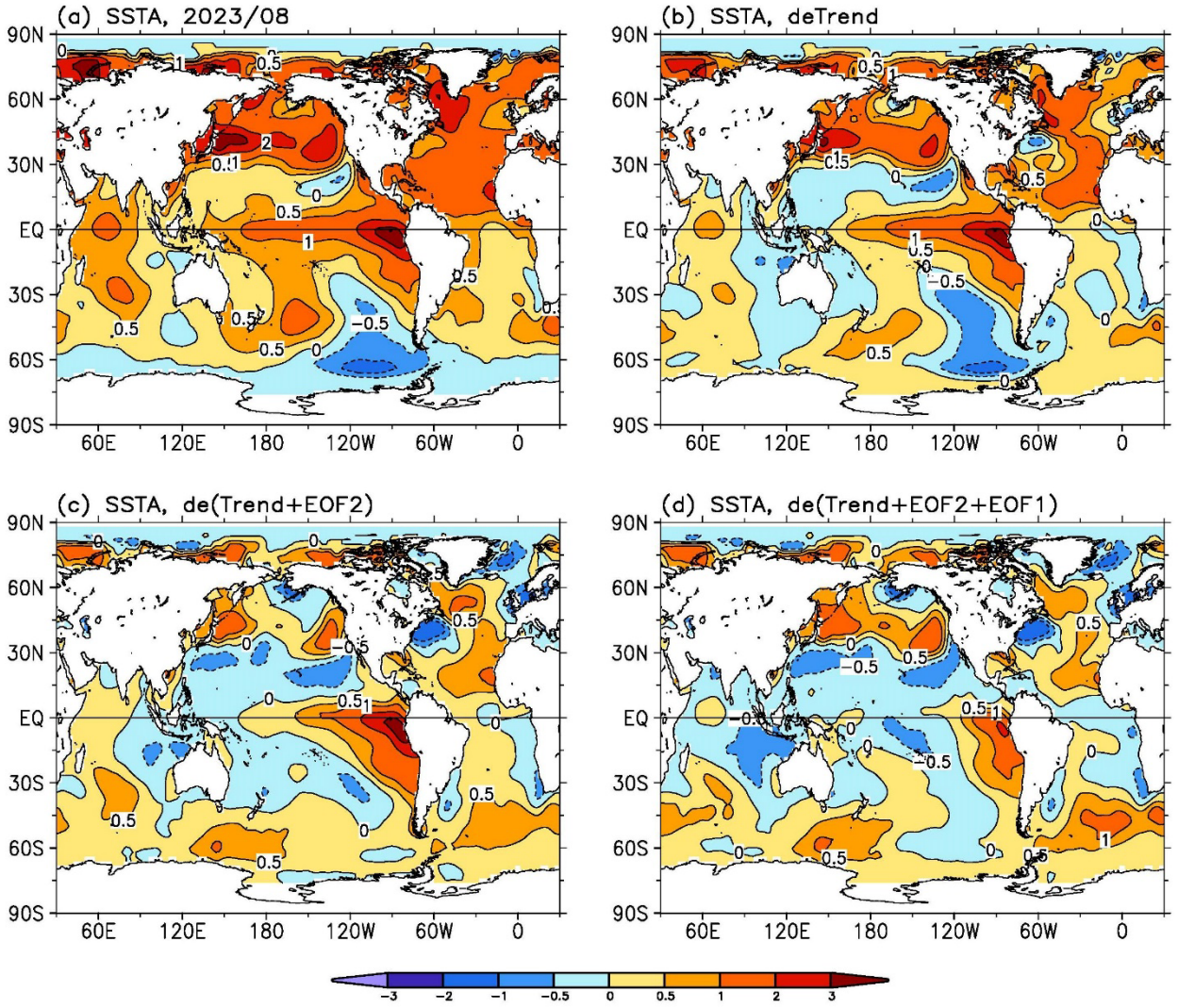

Fig. 5. (a) ERSSTv5 SSTA (ºC) in August 2023, (b) SSTA after removing trend (deTrend), (c) SSTA after removing trend and EOF2 [de(Trend+EOF2)], and (d) SSTA after removing trend, EOF2, and EOF1 [de(Trend+EOF2+EOF1). Globally averaged SSTA variances are 0.59, 0.48, 0.34, and 0.29 in (a), (b), (c) and (d), respectively. Data source: ERSSTv5.

Supporting Information for

Extremely High Sea Surface Temperatures in 2023

Boyin Huang[1], Xungang Yin[1], James A. Carton[2], Ligang Chen[2], Garrett Graham[3], Patrick Hogan[1], Thomas Smith[4], Huai-Min Zhang[1]

[1] NOAA/NCEI, Asheville, North Carolina

[2] Dept. Atmos. Oceanic Science, Univ. Maryland, College Park

[3] North Carolina Institute for Climate Studies, North Carolina State University, Asheville, North Carolina

[4] NOAA/Center for Satellite Applications and Research, College Park, Maryland

Contents of this file

Data Sets and Methods

(a). Data Sets

The NOAA DOISST v2.1 is a global daily SST product with a resolution of 0.25°×0.25º starting from September 1981 (1), which blends in situ SSTs from ships, buoys, Argo floats, and advanced very high resolution radiometer (AVHRR) SST measurements before October 1, 2021. After October 1, 2023, the AVHRR SSTs were replaced by Advanced Clear-Sky Processor for Ocean (ACSPO) (15) SSTs. The AVHRR bias is adjusted according to in situ observations. The ship bias is assumed to be 0.01ºC before June 1, 2023. After June 1, 2023, the constant ship bias was replaced by time dependent monthly ship bias derived from ERSSTv5.

The UK Met Office OSTIA v2 is a daily 0.05º×0.05º SST product starting from 1985 (16). OSTIA includes in situ SSTs from ships and buoys, and satellites. Biases in satellite SSTs in 7º grids are estimated with pairs of in situ SSTs within 25km.

The Canadian Meteorological Centre SST (CMC) v3 is a daily 0.1º×0.1º SST starting from September 1991 (17). CMC v3 uses in situ SSTs from ships and drifting buoys, and satellites. Biases in satellite SSTs in 2.5º grids are estimated with pairs of in situ SSTs within 25km.

The NOAA's Extended Reconstructed SST version 5 (ERSSTv5) (9) is a long-term (starting from 1854) monthly 2º×2º SST product derived from in situ observations from ships, buoys, and Argo floats. The biases of ship SSTs are corrected with reference to nighttime marine air temperature (NMAT) before 1985 and with reference to buoy SSTs after 1985.

The UK Hadley Center Ice and SST (HadISST) (18) is a long-term (starting from 1870) monthly 1º×1º product derived from in situ ships, buoys, and satellite AVHRR observations after the 1980s.

(b) Methods

Using DOISST, the warm SST is quantified by MHWs, which are defined by commonly used criteria (i) SSTAs are higher than the 90th percentile threshold based on 1982–2011 period, and (ii) the high SSTAs are sustained for at least five consecutive days with gaps of less than 3 days (5, 6). To describe the extremeness of the SSTs in 2023, super-MHWs are defined by the SST difference relative to the maximum daily SST (SSTx) climatology over 1982−2022, which are

equivalent to the conventional MHWs but with a 100th percentile threshold without duration limitation as long as SST is higher than SSTx.

To understand the reasons for the extreme SSTs in 2023, the linear trends of SSTAs (relative to 1971−2000) from monthly ERSSTv5 are calculated and filtered out first. The detrended SSTAs are then decomposed into the first two Empirical Orthogonal Functions (EOF1 and EOF2) (7). EOF1 is associated with the El Niño and Southern Oscillation (ENSO) modes at timescale of 3−7 years (8). EOF2 is identified as the Pacific-Atlantic-Arctic Oscillation (PAO) mode in the North Pacific, the North Atlantic, and the Arctic Oceans north of 30ºN, with a period of approximately 70 years. The PAO is similar to the Atlantic Multidecadal Oscillation (AMO) (11, 12), but with a broader spatial distribution across three ocean basins.

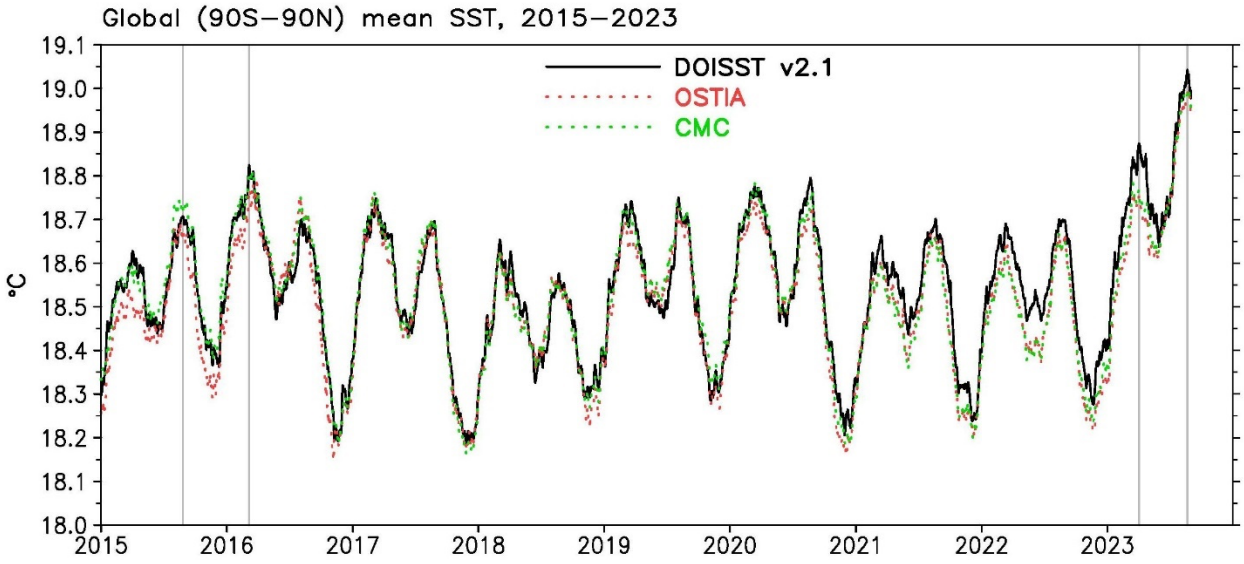

Fig. S1. Globally (90ºS−90ºN) averaged SSTs in DOISST v2.1, OSTIA, and CMC in collocated 0.25º×0.25º grid-boxes. The four vertical lines represent the times when new SST records were set in DOISST on 27 August 2015, 6 March 2016, 4 April 2023, and 21 August 2023. Data source: DOISST v2.1, OSTIA, and CMC.

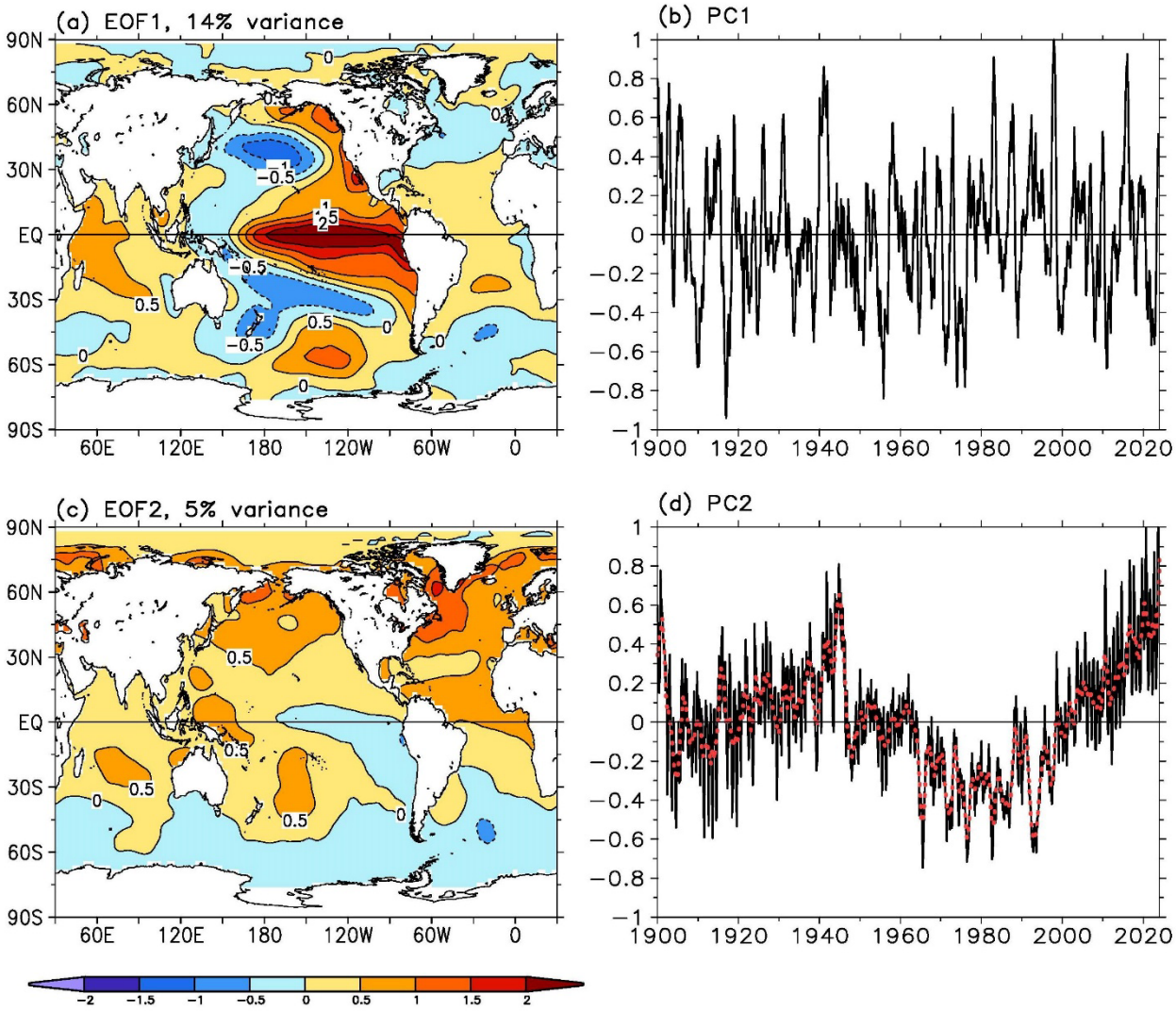

Fig. S2. (a) EOF1, (b) PC1, (c) EOF2, and (d) PC2 of the detrended monthly SSTA of ERSSTv5 from 1900 to 2023. A line (dotted red) with a 12-month filter is overlapped in (d). Data source: ERSSTv5.

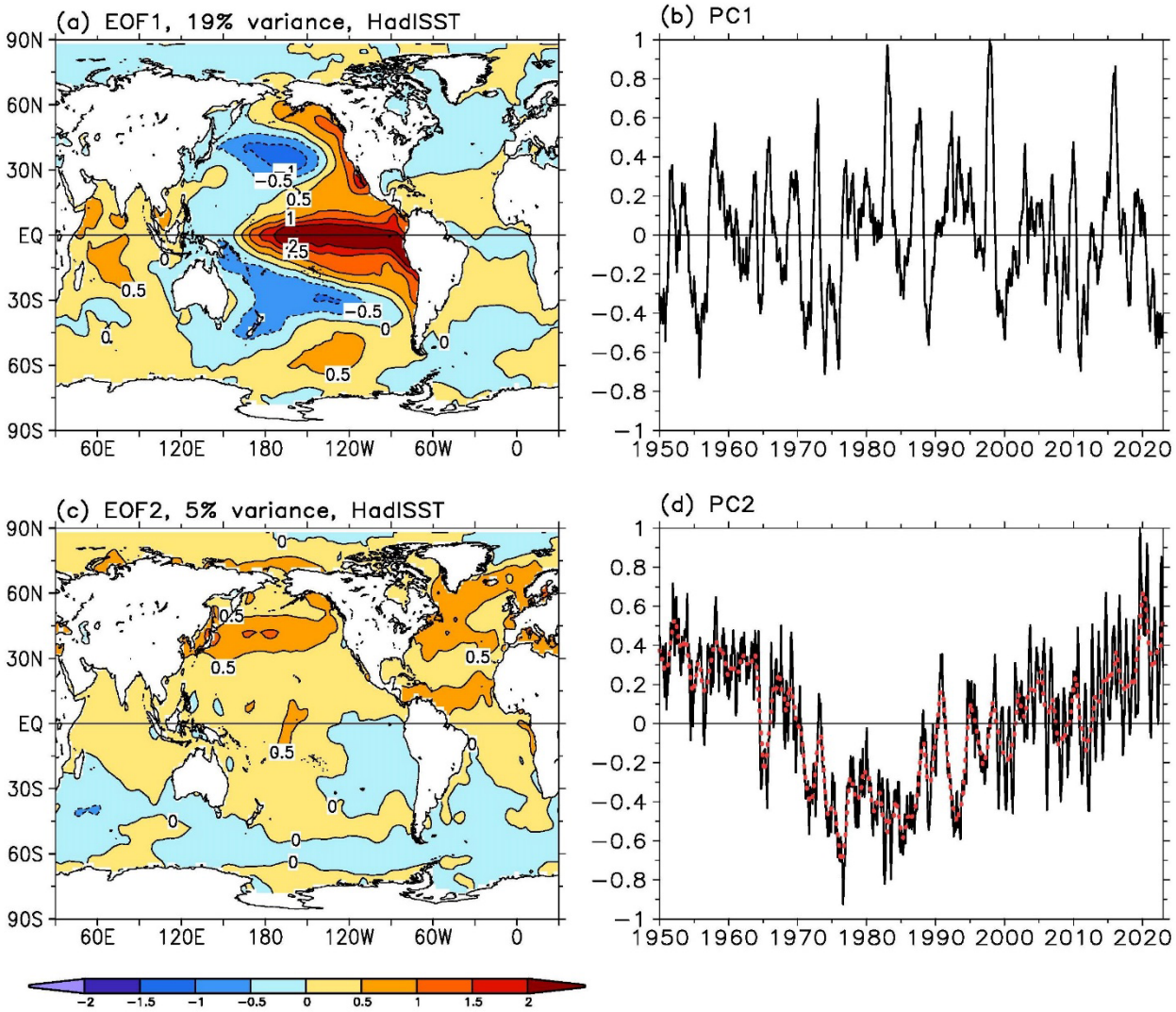

Fig. S3. (a) EOF1, (b) PC1, (c) EOF2, and (d) PC2 of the detrended monthly SSTA of HadISST from 1900 to 2023. A line (dotted red) with a 12-month filter is overlapped in (d). Data source: HadISST from 1950 to 2022.

	SSTA	**deTrend**	**de(Trend+EOF2)**	**de(Trend+EOF2+EOF1)**
North Pacific (30ºN−60ºN)	0.149	0.104, 30%	0.041, 42%	0.036, 3%
North Atlantic (30ºN−60ºN)	0.154	0.090, 42%	0.053, 24%	0.046, 5%
Arctic Ocean (60ºN−80ºN)	0.179	0.101, 44%	0.049, 29%	0.048, 1%
Global Oceans (90ºS−90ºN)	0.060	0.010, 83%	0.007, 5%	0.003, 6%

Table S1. Average (1950−2023) variances (K^2) of ERSSTv5 SSTA (ºC), SSTAs after removing trend (deTrend), removing trend and EOF2 [de(Trend+EOF2)], and removing trend, EOF2, and EOF1 [de(Trend+EOF2+EOF1)] in North Pacific (30ºN−60ºN), North Atlantic (30ºN−60ºN), and Arctic (60ºN−80ºN) as shown in Figure S3. The percentages indicate the contributions of variance changes due to removing trend, EOF2, and EOF1. The variances were calculated without applying 7-month filtering. Data source: ERSSTv5.